Cerqueira, A.; Romero-Gavilán, F.; García-Arnáez, I.; Martínez-Ramos, C.; Ozturan, S.; Iloro, I.; Azkargorta, M.... (2021). Bioactive zinc-doped sol-gel coating modulates protein adsorption patterns and in vitro cell responses. Materials Science and Engineering C. 121:1-10. https://doi.org/10.1016/j.msec.2020.111839

Bioactive zinc-doped sol-gel coating modulates protein adsorption patterns and *in vitro* cell responses

MSc. A. Cerqueira[1#], Dr. F. Romero-Gavilán[1*#], MSc. I. García-Arnáez[2], Dr. C. Martinez-Ramos[3], Prof. S. Ozturan[4], Dr. I. Iloro[5], Dr. M. Azkargorta[5], Prof. F. Elortza[5], Prof. R. Izquierdo[1], Prof. M. Gurruchaga[2], Prof. I. Goñi[2], Prof. J. Suay[1]

[1]Department of Industrial Systems Engineering and Design, Universitat Jaume I, Av. Vicent Sos Baynat s/n, 12071 Castellón de la Plana, Spain

[2]Departament of Science and Technology of Polymers, Universidad del País Vasco, P. M. de Lardizábal, 3, 20018 San Sebastián, Spain

[3]Center for Biomaterials and Tissue Engineering, Universitat Politècnica de Valencia, Camino de Vera, s/n 46022 Valencia, Spain

[4]Department of Periodontology, Faculty of Dentristy, Istanbul Medeniyet University, Istanbul, Turkey

[5]Proteomics Platform, CIC bioGUNE, Basque Research and Technology Alliance (BRTA), CIBERehd, ProteoRed-ISCIII, Bizkaia Science and Technology Park, 48160 Derio, Spain

[#]Co-authorship

*Corresponding author: Francisco Romero-Gavilán

Departamento de Ingeniería de Sistemas Industriales y Diseño

Campus del Ríu Sec

Avda. Vicent Sos Baynat s/n

12071 – Castelló de la Plana (España)

E-mail: gavilan@uji.es

No conflicts of interest are declared.

Keywords

Proteomics, Bioinorganic Chemistry, Biomaterials, Bone Regeneration, Hybrids

Abstract

Zinc is an essential element with an important role in stimulating the osteogenesis and mineralization and suppressing osteoclast differentiation. In this study, new bioactive $ZnCl_2$-doped sol-gel materials were designed to be applied as coatings onto titanium. The biomaterials were physicochemically characterized and the cellular responses evaluated *in vitro* using MC3T3-E1 osteoblasts and RAW264.7 macrophages. The effect of Zn on the adsorption of human serum proteins onto the material surface was evaluated through nLC-MS/MS. The incorporation of Zn did not affect the crosslinking of the sol-gel network. A controlled Zn^{2+} release was obtained, reaching values below 10 ppm after 21 days. The materials were no cytotoxic and lead to increased gene expression of ALP, TGF-β, and RUNX2 in the osteoblasts. In macrophages, an increase of IL-1β, TGF-β, and IL-4 gene expression was accompanied by a reduced TNF-α liberation. Proteomic results showed changes in the adsorption patterns of proteins associated with immunological, coagulative, and regenerative functions, in a Zn dose-dependent manner. The variations in protein adsorption might lead to the downregulation of the NF-κB pathway, thus explain the observed biological effects of Zn incorporation into biomaterials. Overall, these coatings demonstrated their potential to promote bone tissue regeneration.

1. Introduction

As an essential trace element, zinc plays an important physiological role in the human body, performing various functions in growth, immunity, tissue maintenance, and wound healing [1]. Most of the zinc is stored in bone tissue, mainly as a component of the calcified matrix [2]. It plays a pivotal role in bone metabolism and remodeling [3], supports osteoblastogenesis, and suppresses osteoclastogenesis [4]. Zinc can enhance osteogenesis and mineralization by activating the aminoacyl-RNA synthesis in osteoblastic cells [5] and stimulating the alkaline phosphatase and collagen synthesis in a dose-dependent manner [6]. However, this divalent cation can also downregulate osteoclast differentiation due to its effect on the RANKL/RANK/OPG signaling pathway [7]. Zinc deficiency causes various diseases and skeletal abnormalities during fetal and postnatal development, such as bone growth retardation, abnormal mineralization, and osteoporosis [8]. Zinc is also known for its antioxidant and anti-inflammatory properties; it is used as a therapeutic agent in chronic diseases [9]. Moreover, Zn inhibits the induction of TNF-α and IL1-β in monocyte macrophages and prevents the TNF-α-induced NF-κB activation [10].

The intrinsic physiological relevance of this element has attracted the interest of researchers in the biomaterial field; its incorporation into bone-engineering materials could enhance the desired regenerative properties. Zn-doped degradable materials such as hydroxyapatites, bioglasses, and metallic alloys have recently emerged demonstrating pro-regenerative capabilities [11]. However, delayed osseointegration induced by excessive release of Zn^{2+} ions has been observed in pure Zn-ion implants [5]. Thus, the control of the degradation product release is necessary to ensure the biosafety of these materials and optimize their therapeutic effects [12].

Immediately after implantation, a biomaterial interacts with surrounding tissues and fluids. A complex sequence of events is initiated in a cascade. These events are oriented primarily towards the tissue repair and integration or rejection of the introduced foreign body [13,14]. One of the first steps in this process is the interaction between the biomaterial and body fluids, such as the blood. As a result, many proteins adhere to the surface of the implant, using a competitive displacement mechanism known as the Vroman effect [15]. Regenerative biological processes triggered by implantation, such as inflammation, coagulation, fibrinolysis, and angiogenesis, will depend on the type of proteins attached to the biomaterial [16,17]. Inflammation, which is one of the first reactions to implantation, is the pivotal process in tissue regeneration and can

condition the subsequent responses to the implant [16,18]. Depending on the intensity of the inflammatory response, it can initiate a regeneration process, recruiting the mesenchymal cells and boosting osteogenesis, or can trigger a foreign body reaction causing the implant rejection [19,20].

This study aimed to synthesize and characterize a new organic-inorganic sol-gel release vehicle doped with Zn ions to be applied as coatings onto titanium. The materials were physiochemically characterized and the effects of Zn^{2+} on protein adsorption were studied using proteomic analysis. Also, *in vitro* assays of cell behavior were conducted using MC3T3-E1 osteoblast and RAW 264.7 macrophage cell lines. The correlation between the cellular responses and the Zn dose-dependent protein adsorption patterns will allow to better understand the role of this element in bone tissue regeneration.

2. Results

2.1. Physicochemical characterization

The organic-inorganic sol-gel materials with increasing amounts of $ZnCl_2$ were successfully synthesized and applied as coatings onto the Ti discs. As can be seen in SEM micrographs (**Figure 1**), no cracks or holes resulting from the curing process were detected. Moreover, no salt precipitates were observed, so the $ZnCl_2$ was correctly incorporated into the sol-gel network.

The obtained sol-gel materials were chemically characterized using ^{29}Si-NMR and FT-IR (**Figure 2**). The ^{29}Si-NMR spectra showed no effects on the silica network condensation with the $ZnCl_2$ addition (**Figure 2a**). The signals detected in the range between -50 and -70 ppm can be assigned to the MTMOS trifunctional precursor (T units - $CH_3{\cdot}SiO_3$). The signals between – 97.5 and -115 ppm represent the TEOS tetrafunctional alkoxysilane (Q units - SiO_4) [21]. Thus, the signals at -56 and -66 ppm indicate the presence of T^2 and T^3 species, while chemical shifts at -102 and -110 ppm can be associated with the formation of Q^3 and Q^4 structures, respectively [22]. In general, the networks reached a high degree of MTMOS crosslinking as T^3 signal was more intense than T^2, and no T^0 or T^1 shifts were observed. Similarly, no Q^0, Q^1 or Q^2 TEOS species were identified although, in this case, the level of condensation was probably lower as Q^3 peak was larger than Q^4. The FT-IR results are displayed in **Figure 2b**. Bands at 780, 1020 and 1125 cm^{-1} associated with the polysiloxane chain vibration reveal the formation of Si-O-Si bonds during the sol-gel synthesis [23]. The band at 950 cm^{-1} indicates the presence of non-condensed Si-OH species [24]. The methyl group integrity in the sol-gel structure is confirmed

by its characteristics bands at 1265 and 2980 cm^{-1}, which are attributed to the Si-C and C-H bonds, respectively [23].

The surface roughness was evaluated using the Ra parameter. **Figure 3a** shows that the incorporation of $ZnCl_2$ into the coatings did not change their Ra values (in comparison with the material without Zn) significantly. **Figure 3b** displays the contact angle measurements. The addition of $ZnCl_2$ to the MT network, resulting in the reduction in surface hydrophilicity, caused a significant increase in the contact angle values.

The hydrolytic degradation kinetics of the tested sol-gel materials are shown in **Figure 4a**. In general, all the formulations showed the highest mass-loss rates during the first week of incubation in water. Nevertheless, their degradation increased throughout the test period (63 days); reaching mass loss values of approximately 40 % of the initial mass. The hydrolytic degradation of sol-gel coatings intensified with an increase in $ZnCl_2$ content. A continuous release of Zn^{2+} was observed until the end of the assay, at 21 days (**Figure 4b**). The largest amounts of Zn^{2+} were released from the material with the highest proportion of $ZnCl_2$ in the MT network.

2.2. *In vitro* assays

2.2.1. Osteogenic responses: effects on osteoblastic cells

None of the materials tested were cytotoxic (data not shown). In tests of cell proliferation, a peak in cell growth was observed after 3 days in all cases, but no significant differences were found for any of the studied coatings (**Figure 5a**). The mineralization levels, evaluated by examining the ALP activity, showed a significant increase for MT0.5Zn after 7 days, in comparison with the MT. After 14 days, there was a general increase in the ALP activity; however, it was significantly lower for the MT1Zn and MT1.5Zn materials in comparison with the MT (**Figure 5b**).

To evaluate how Zn-enriched sol-gel coatings affect osteogenesis, gene expression was measured in MC3T3-E1 cells (**Figure 6**). An increase in TGFβ expression was observed on MT1.5Zn coating after 7 days (**Figure 6b**). After 14 days, there was an increase in ALP expression on MT1.5Zn and TGFβ expression levels on MT0.5Zn and MT1.5Zn coatings (**Figure 6a and 6b)**. In what concerns iNOS (**Figure 6c**), an increase of these markers was detected at 7 days in MT0.5Zn and MT1.5Zn, while MT1Zn showed a significant decrease. After 14 days, this marker was increased in MT1Zn and MT1.5Zn. In the markers related to

osteoclastogenesis, RUNX2 showed an increase in MT1Zn and MT1.5Zn at 7 days (**Figure 6d**), while MT1.5Zn lead to an increase of RANK in the same time point (**Figure 6f**). At 14 days, RUNX2 was significantly more expressed in MT1.5Zn. RANKL expression showed no differences between materials (**Figure 6e**).

2.2.2. Inflammatory responses: effects on macrophages

Gene expression of RAW264.7 was examined to evaluate the effects of Zn-enriched sol-gel coatings on inflammatory-response markers (**Figure 7**). After 2 days of incubation, there were no changes in pro- or anti-inflammatory marker levels with Zn-coatings, except in IL-1β, which presented a significant increase in MT1.5Zn (**Figure 7b**). After 4 days, there was a significant increase in TNF-α and IL-1β gene expression on MT1.5Zn (**Figures 7a and b**). An increase in the expression of TGFβ was seen on all the tested materials (**Figure 7c**), while IL-4 showed an increase in MT0.5Zn and MT1.5Zn. The production of TNF-α by RAW264.7 cells was measured using ELISA (**Figure 7e**). For the first two days, there were no differences between the materials. After 4 days, there was a significant decrease in TNF-α production on Zn-coatings (MT0.5Zn and MT1Zn) in comparison with the MT.

2.2.3. Proteomic analysis

A total of 289 distinct proteins were identified in the elutions of the protein layers adsorbed onto the different materials. The comparative analysis using PEAKS detected 61 proteins differentially adsorbed onto the materials enriched with Zn (**Supplementary Table 1**). PANTHER and DAVID proteomic tools were employed to classify these proteins by their functions. The differentially adsorbed proteins and their functions associated with the regeneration process are listed in **Table 1**. Proteins associated with innate immunity and inflammation were detected in higher proportions on the surfaces with Zn. These were SAMP, CO4A, CO9, CXCL7, CO3, C1S, CO4B and immunoglobulins LAC3, IGJ, and IGKC, as well as FHR1, CLUS, IC1, and VTNC, which have regulatory/anti-inflammatory functions. A cluster of apolipoproteins, linked to lipid metabolism functions, also preferentially adsorbed onto Zn-containing coatings (APOF, APOL1, SAA4, APOC4, APOC3, APOC2, APOA2, and APOA1). HBB showed increased adsorption to MT0.5Zn and MT1Zn, while reduced amounts of HRG adhered to MT0.5Zn. These two proteins are associated with metal-binding and blood-clotting functions. Similarly, PLF4, PROC, and IPSP proteins, which showed increased affinity to the Zn-containing coatings, were linked to blood coagulation processes. VTNC was found more adsorbed to all the Zn-coatings than to the control surface. This glycoprotein is associated

with regenerative functions, but also to blood clotting and the inhibition of immune response. In contrast, TITIN, a metal-binding protein with tissue regeneration functions, showed weakened adsorption onto MT0.5Zn. However, TITIN showed an augmented affinity to the coating doped with 1 % $ZnCl_2$. CERU and KAIN glycoproteins were most abundant on the coating with the highest amount of Zn. CERU is associated with metal-binding, while KAIN is a protease inhibitor. PRDX1, which has a peroxidase activity, showed a weakened affinity to the MT1Zn material, whereas CATB, associated with proteolysis, was less abundant on MT1.5Zn.

The proteomic tool PANTHER was used to classify the differentially adsorbed proteins according to their participation in biological processes (**Figure 8**). The proteins with increased adsorption to the Zn-containing coatings are associated with a wide range of different processes (such as biological regulation, response to a stimulus, developmental, locomotion, metabolic, cellular, multicellular, localization, biogenesis, signaling and immune system processes). In contrast, the proteins with reduced affinity to the Zn-coatings are mainly related to the response to stimulus, biological regulation, and metabolic, cellular and multicellular functions in biological processes. The biological adhesion and immune system functions were also associated with some of the proteins with reduced affinity to the MT1Zn material.

3. Discussion

The main aim of this study was to develop and characterize a new bioactive Zn-doped sol-gel coating for a Ti substrate. The effects of this element on protein adsorption and cellular responses in terms of osteogenesis and inflammation were evaluated. Zinc is an essential trace element with a stimulatory effect on bone growth and a pivotal role in bone maintenance. It has been described as the 'calcium of the twenty-first century' since Zn-containing biomaterials are showing great promise in applications for bone tissue regeneration [12].

The Zn-doped sol-gel coatings were obtained following the sol-gel route. The incorporation of this compound did not affect the degree of crosslinking in the new sol-gel network or caused significant differences in surface roughness of the new coatings. However, increasing the amount of Zn in the sol-gel resulted in a significant reduction of the material hydrophilicity. The material without Zn lost approximately 40 % of its mass after 63 days of incubation in water. The incorporation of $ZnCl_2$ increased the hydrolytic degradation rate; the MT1.5Zn composition lost around 50 % of its mass after the same period. A controlled Zn^{2+} release was achieved as more Zn salt was incorporated into the network; the more Zn was liberated. The

release of this compound continued until the end of the essay (21 days), demonstrating consistent long-term release properties. The quantified Zn^{2+} concentrations were less than 10 ppm in all the cases, not reaching the limit of cellular toxicity of 26.2 ppm defined by Brauer *et al.* [25]. Moreover, *in vitro* results showed that these new Zn-containing coatings were not cytotoxic to MC3T3-E1 cells.

The analysis of MC3T3-E1 osteogenic markers showed that RUNX2 expression, a member of the runt domain family involved in bone development, was increased at 7 and 14 days. Yamaguchi *et al*. [26] showed zinc sulphate upregulates the RUNX2 expression. This was accompanied by the augmented ALP expression at 14 days in MT1.5Zn, whose activity is activated by RUNX2 [27] and stimulated by Zn in MC3T3-E1 cells [6]. Additionally, TGF-β gene expression was increased on MT0.5Zn and MT1.5Zn. This cytokine is critical in the promotion of bone formation, as it plays roles in the recruitment of osteoblast, and enhancement of osteoblast proliferation and differentiation [28], thus confirming the effects of these Zn-doped coatings in the osteoblastic differentiation.

Inflammation is required to protect the host from tissue damage, which leads to the restoration of homeostasis. The pro-inflammatory markers TNF-α and IL-1β [29] presented an increased gene expression in MT1.5Zn after 4 days of culture, while, at the same time point, MT0.5Zn and MT1Zn secreted significantly less TNF-α. Similarly, Giovanni *et al.* [30] developed zinc oxide nanoparticles that lead to an increased fold change in TNF-α and IL-1β in a dose-response manner. On the other hand, the overexpression of TGF-β and IL-4 [29], two anti-inflammatory markers, in Zn-containing materials, confirming that the inflammatory responses might depend on the used Zn concentration.

The phenomenon of protein adsorption onto a material can affect the initial biological healing processes [31]. Therefore, studying how proteins are attached to a surface can help to predict a biomaterial outcome. The nLC-MS/MS analysis identified significant changes in the patterns of proteins adsorbed associated with increasing amounts of Zn incorporated onto the sol-gel coating. Among the proteins found, a set belonging to a cluster related to the innate immune system was identified, containing immunoglobulins and complement system proteins such as C1S, CO3, CO4A, CO4B and CO9, which can activate the cascade of pro-inflammatory response [19]. In general, these proteins tended to increase their attachment affinity to the surfaces as more Zn was added to the sol-gel. However, a clear increase in the adsorption of proteins associated with inhibitory/regulatory functions of complement cascade was also

observed. Proteins such as VTNC, IC1, FHR1, and CLUS, which showed augmented affinity to Zn-enriched coatings, can control the complement system activation. They act as anti-inflammatory factors [32]. The increased adsorption of this group of proteins is consistent with the anti-inflammatory potential observed *in vitro*. Likewise, the increased attachment of apolipoproteins onto the materials with Zn could affect the immune response regulation. This protein family can prevent the initiation of innate immune response by inhibition of NF-κB-dependent gene expression [33].

Moreover, the VTNC can promote the macrophage polarization into the M2 pro-regenerative phenotype [34]. This protein is associated with the coagulation system; it contributes to thrombus formation and participates in vascular homeostasis and tissue regeneration [35]. VTNC is also involved in bone metabolism as it can promote the osteogenic differentiation of mesenchymal stem cells [36]. It improves the bone healing capacity of Ti implants [37] and the biomaterial vascularization process [38]. The rise in VTCN adsorption with increasing Zn content in the coatings might be correlated with their increased osteogenic activity. Moreover, TITIN, more abundant on the MT1Zn, has been associated with signaling in bone remodeling. It has also been linked with an increase in cell proliferation of MG-63 osteoblasts via activation of the Wnt/β-catenin pathway [39]. Similarly, CXCL7, preferentially adsorbed onto MT1.5Zn, can significantly stimulate the recruitment of human mesenchymal stem cells (MSC) *in vitro* [40].

The studies of the role of Zn^{2+} in bone resorption have revealed that the osteoclasts are sensitive to this ion; a significant decrease in bone resorption occurs at the concentration as low as 10^{-14} M [41]. Binding of RANKL to its receptor RANK activates NF-kB, inducing osteoclast differentiation. Zn^{2+} may reduce osteoclastogenesis via suppression of RANK expression through prevention of oxidative stress species production [7]. In this study, no differences in the expression RANKL were found. Similarly, Yusa et *al.* found that Zn did not affect RANKL or OPG mRNA expression in zinc-modified titanium surfaces [27], which is consistent with these results. However, RANK expression increased for MT1.5Zn; in parallel iNOS marker resulted overexpressed for MT1Zn and MT1.5Zn. Thus, the effect of Zn-enriched materials on osteoclastogenesis could depend on the added Zn concentration.

The proteomic results indicate that Zn could also affect the coagulation processes around the implant materials. The proteins with pro-coagulant (VTNC, PLF4, IPSP, and HBB) and anti-coagulant functions (PROC) showed increased adsorption to Zn-containing surfaces, in a Zn dose-dependent manner. It is difficult to predict the real-life effect of these proteins on the

implant surface. Some studies have described a potential anticoagulation role of Zn-alloy biomaterials [42,43]. However, it has also been reported that high concentrations of Zn^{2+} might promote thrombosis [43].

Interestingly, CERU, an acute-phase protein with antioxidant properties, showed increased adsorption to the surfaces with Zn (a 21-fold increase on the MT1.5Zn material in comparison with the control surface). This protein is known as the main warehouse of plasma copper, but it can also bind to Zn via its copper-binding sites [44]. Its augmented adsorption in MT1.5Zn supports these findings. High levels of CERU in plasma have been associated with osteoporosis, independently of other inflammatory parameters [45]. However, its role in this bone disease is unknown. KAIN, which belongs to the serine proteinase inhibitor superfamily, was also significantly more abundant on the MT1.5Zn surface. This protein exerts its anti-inflammatory effect via the canonical Wnt pathway [46]. It can stimulate the M2 phenotype in cultured RAW 264.7 macrophages, causing overexpression of IL-10 [47]. However, KAIN plays a dual role in angiogenesis. It inhibits the process by blocking VEGF-induced effects and TNF-α-induced VEGF synthesis, but it can also stimulate neovascularization by increasing the levels of endothelial nitric oxide synthase (eNOS) and VEGF [48].

The adsorption of the proteins CATB and PRDX1 was reduced on the MT1.5Zn and MT1Zn surfaces (33-fold and 25-fold decrease), respectively. The peroxidase PRDX1 is associated with various biological processes such as the detoxification of oxidants and cell apoptosis. Du *et al.* have reported that the association between oestrogen and this protein might affect the osteoblast cell responses to oxidative stress [49]. CATB is an enzyme involved in promoting chronic inflammation, delaying tissue healing [50]. This protein is also responsible for NF-kB activation via autophagy degradation of IkBα in microglia/macrophages [51]. Moreover, elevated levels of CATB are typically observed in many chronic inflammatory diseases, including rheumatoid arthritis and periodontitis [52,53]. Thus, its diminished affinity to Zn-containing biomaterials might have a positive effect on tissue regeneration.

4. Conclusion

New sol-gel materials doped with increasing amounts of Zn were applied as coatings onto Ti discs, allowing the control of the release kinetics of this ion. The presence of Zn affected the *in vitro* responses of osteoblasts and macrophages and protein adsorption onto the coated surfaces. The levels of ALP, TGF-β, and RUNX2 gene expression in osteoblasts increased for the materials with Zn, showing the osteogenic potential of these materials. The fold-changes in

TNF-α, IL-1β, TGF-β and IL-4 show that the inflammatory responses these are dependent on the amount of Zn is incorporated into the material. The nLC-MS/MS proteomic analysis revealed that the addition of Zn significantly changed the attachment of proteins involved in the immune, coagulation, and regenerative processes. Zinc sharply increased the adsorption of proteins regulating the immune reaction, such as VTNC, IC1, FHR1, CLUS, and KAIN. In contrast, it decreased the adsorption of CATB protein, which is associated with chronic inflammation and delayed healing. Moreover, an increased proportion of proteins with osteogenic function, such as VTNC, attached to the Zn-containing coatings. Thus, the proteomic results were consistent with the biological responses observed *in vitro*. Our results show the future possibility of clinical application of these new coatings to bioactivate Ti prostheses.

5. Materials and methods

5.1. Substrate

Grade- 4 Ti discs, 1-mm thick, 12 mm in diameter (Ilerimplant-GMI SL., Lleida, Spain), were employed as a substrate for the coatings. Disc surfaces were first modified using the sandblasting and acid-etching treatment (SAE) described in the previous study [54] and sterilized with UV radiation.

5.2. Sol-gel synthesis and coating preparation

The Zn-containing hybrid materials were developed using the sol-gel synthesis. Organically modified alkoxysilanes, methyltrimethoxysilane (MTMOS; M) and tetraethyl orthosilicate (TEOS; T), were employed as precursors. The proportion of these reagents was 70 % of M to 30 % of T (molar ratio), as described in previous studies [55]. The solvent used in the synthesis was 2-Propanol (volume ratio of alcohol to siloxane, 1:1). The precursor hydrolysis was conducted by adding the corresponding stoichiometric amount of H_2O at a rate of 1 drop s^{-1}. The water was acidified with HNO_3 (0.1 M) to catalyze the sol-gel reactions. An appropriate amount of $ZnCl_2$ was dissolved in this solution for its incorporation into the sol-gel mixture. The preparations were kept for 1 h under stirring and then 1 h at rest at room temperature. Four different compositions were synthesized: the sol-gel network without Zn (MT; control) and enriched with 0.5, 1, and 1.5 wt % $ZnCl_2$ (designated as MT0.5Zn, MT1Zn, and MT1.5Zn, respectively). The mass percentages were relative to the total amount of alkoxysilane. Also, SAE uncoated titanium samples (Ti) were used as controls. All the reagents employed for the synthesis were purchased from Sigma-Aldrich (Merck KGaA, Darmstadt, Germany). The

samples were prepared immediately after finishing the sol-gel synthesis. The coatings were applied onto the SAE-Ti discs with a dip-coater (KSV DC; KSV NIMA, Espoo, Finland). The discs were immersed in the sol-gel solutions at a speed of 60 cm min^{-1}, left immersed for one minute, and removed at a 100 cm min^{-1}. To evaluate the hydrolytic degradation and Zn^{2+} release, glass slides were used as a substrate for the coatings. The glass surfaces were first cleaned with HNO_3 solution (25 % v/v) in an ultrasonic bath (Sonoplus HD 3200) for 20 min at 30 W. A second wash with distilled water was performed under the same conditions. Then, the samples were coated by casting, adding the same amount of sol-gel in all cases. To carry out the chemical analyses, free films of the materials were obtained by pouring the sol-gel solutions into non-stick Teflon molds. Finally, all the samples were cured for 2 h at 80 °C.

5.3. Physicochemical characterization

The morphology of the obtained coatings was analyzed using SEM with a Leica-Zeiss LEO equipment, under vacuum (Leica, Wetzlar, Germany). Platinum sputtering was used to increase the coating conductivity for the SEM examination. Fourier-transform infrared spectroscopy (FTIR; Thermo Nicolet 6700 spectrometer, Thermo Fisher Scientific, Waltham, MA, USA) with an attenuated total reflection system (ATR) was employed for chemical characterization of the synthesized materials. The spectra were recorded in the 400 to 4000 cm^{-1} wavelength range. The level of structural crosslinking was studied using silicon solid-state nuclear magnetic resonance spectroscopy (^{29}Si-NMR). To achieve this, a Bruker 400 Avance III WB Plus spectrometer (Bruker, Billerica, MA, USA) with a cross-polarization magic-angle spinning (CP-MAS) probe for solid samples was employed. The pulse sequence for the analysis was the Bruker standard: 79.5 MHz frequency, 55 kHz spectral width, 2 ms contact time and 5 s delay time. The spinning speed was 7.0 kHz. The surface roughness of the developed coatings was measured using an optical profilometer (interferometric and confocal) PLm2300 (Sensofar, Barcelona, Spain). Three discs were tested for each condition. Three measurements were performed for each disc to obtain an average Ra (arithmetic average roughness parameter).

The wettability was characterized using contact angle measurements, employing an automatic contact angle meter OCA 20 (Dataphysics Instruments, Filderstadt, Germany). Drops of 10 μL of ultrapure water were deposited on the material surfaces at a 27.5 μL s^{-1} dosing rate. Contact angles were determined using SCA 20 software (DataPhysics Instruments). Six discs of each material were studied, after depositing two drops on each disc.

Hydrolytic degradation of the coatings was examined by measuring the sol-gel mass loss after incubation in 50 mL of distilled water at 37 °C for 7, 14, 28, 49, and 63 days. The degradation of the coatings was registered as the percentage of the original mass lost. Three different samples were used for each condition. The Zn^{2+} release kinetics were measured using an inductively coupled plasma mass spectrometer (Agilent 7700 Series ICPMS; Agilent Technologies, Santa Clara, CA, USA). Samples were incubated in ddH_2O at 37 °C for 21 days. Aliquots of 0.5 mL were removed after 2, 4, 8, 168, 336, and 504 h of immersion. Each data point is the average of three individual measurements.

5.4. *In vitro* assays

5.4.1. Cell culture

Mouse calvaria osteosarcoma (MC3T3-E1) cell line was cultured on the discs at a concentration of 1.75×10^4 cells cm^{-2} for 7 and 14 days. For the first 24 h, the culture medium was composed of low-glucose DMEM (Gibco, Thermo Fisher Scientific) supplemented with 1 % penicillin/streptomycin (Biowest Inc., Riverside, MO, USA) and 10 % FBS (Gibco). The samples were kept in a cell incubator (90 % humidity, 37 °C, 5 % CO_2). Then, the cell culture medium was replaced with osteogenic medium (DMEM, 1 % of penicillin/streptomycin, 10 % FBS, 1 % ascorbic acid (5 mg mL^{-1}), and 0.21 % β-glycerol phosphate), which was changed every two days.

Mouse murine macrophage (RAW264.7) cell line was cultured on the materials at a concentration of 30×10^4 cells cm^{-2} for 2 and 4 days in high-glucose DMEM supplemented with 1 % penicillin/streptomycin and 10 % FBS in a cell incubator (90 % humidity, 37 °C, 5 % CO_2).

5.4.2. Cytotoxicity, proliferation, and ALP activity

To evaluate the cytotoxicity of biomaterials, the ISO 10993-5:2009 (Annex C) norm [56] was followed. Samples were prepared according to the ISO 10993-12:2012 norm [57]. MC3T3-E1 cells were seeded and incubated in 96-well NUNC plates (Thermo Fisher Scientific) for 24 h. For serum extraction, the materials were incubated in cell culture medium for the same period. Then, the cells were exposed to the material extract for another 24 h. Based on the formazan formation, the CellTiter 96® Proliferation Assay (MTS; Promega, Madison, WI) was used according to manufacturer's guidelines. The negative control was composed of wells with only cells and the cells incubated with latex (cytotoxic compound) constituted the positive control. A material would be considered cytotoxic if the cell viability fell below 70 %.

To measure the effects of the tested biomaterials on proliferation, MC3T3-E1 cells were cultured on the discs for 1, 3, and 7 days and the alamarBlue™ cell viability reagent (Invitrogen, Thermo Fisher Scientific) was used following the manufacturer's protocol.

The ALP activity was measured, following the protocol of Araújo-Gomes *et al.* [19], to evaluate the effect of the Zn-enriched materials on cell mineralization. Briefly, the MC3T3-E1 cells were seeded onto different disc surfaces in 48-well NUNC plates (Thermo Fisher Scientific). After culturing for 7 and 14 days, lysis buffer (0.2 % Triton X-100, 10 mM Tris-HCl, pH 7.2) was added. Then, 100 µL of *p*-NPP (1mg mL^{-1}) in substrate buffer (50 mM glycine, 1 mM $MgCl_2$, pH 10.5) was added to the samples. After 2 h of incubation, the absorbance at 405 nm was measured using a microplate reader. The ALP activity was obtained using the standard curve of *p*-nitrophenol in 0.02 mM sodium hydroxide. It was normalized to protein content obtained employing a Pierce BCA assay kit (Thermo Fisher Scientific).

5.4.3. Cytokine quantification by ELISA

The level of tumor necrosis factor (TNF-α) was measured in the culture medium of RAW264.7 cells incubated on the discs for 2 and 4 days. Its concentration was determined using an ELISA (Invitrogen, Thermo Fisher Scientific) kit following the manufacturer's instructions.

5.4.4. Relative gene expression: RNA extraction, cDNA synthesis, and qRT-PCR

For total RNA extraction, MC3T3-E1 cells were grown on the tested materials for 7 and 14 days, and RAW264.7 for 2 and 4 days. The assays were carried out in 48-well NUNC plates (Thermo Fisher Scientific). At each time point, RNA was extracted using TRIzol as described in Cerqueira *et al.* [58]. RNA concentration, integrity, and quality were measured employing NanoVue® Plus spectrophotometer (GE Healthcare Life Sciences, Little Chalfont, UK).

For cDNA synthesis, approximately 1 µg of total RNA was converted into cDNA using PrimeScript RT Reagent Kit (Perfect Real-Time; TAKARA Bio Inc., Shiga, Japan). The reaction was carried out under the following conditions: 37 °C for 15 min, 85 °C for 5 secs, and a final hold at 4 °C. The resulting cDNA was diluted in DNase-free water to a concentration suitable for gene expression evaluation. Quantitative real-time PCR (qRT-PCR) was carried out in 96-well plates (Applied Biosystems®, Thermo Fisher Scientific) for the genes of interest and the housekeeping gene (*GAPDH*). Primers were designed using PRIMER3plus software tool from sequences obtained from NCBI Nucleotide and purchased from Thermo Fisher Scientific. Targets are shown in **Table 2**. Individual qRT-PCR reactions contained 1 µL of cDNA, 0.2 µL

of specific primers (forward and reverse, at 10 µM concentration) and 5 µL of SYBR Premix Ex Taq (Tli RNase H Plus; TAKARA), in a final volume of 10 µL. Reactions were carried out in a StepOnePlus™ Real-Time PCR System (Applied Biosystems®, Thermo Fisher Scientific). Fold changes were calculated using the $2^{-\Delta\Delta Ct}$ method and data normalized to the wells without any material.

5.4.5. Protein layer elution and proteomic analysis

The protein layers on the distinct sol-gel formulations were examined after their incubation in a humidified atmosphere (37 °C, 5 % CO_2) for 3 h with 1 mL of human blood serum from male AB plasma (Sigma-Aldrich). The serum was removed, and non-adsorbed proteins were eliminated by five consecutive washes with ddH_2O and another with 100 mM NaCl, 50 mM Tris-HCl, pH 7.0. The adsorbed proteins were eluted by washing the surfaces with 0.5 M triethylammonium bicarbonate buffer (TEAB), with 4 % sodium dodecyl sulfate (SDS) and 100 mM-dithiothreitol (DTT). The experiment was performed in quadruplicate for each material, and each of these replicas was the result of pooling four different processed samples. The total protein content of the serum was measured before the assay, obtaining a value of 51 mg mL^{-1}.

The eluted proteins were characterized using electrospray tandem mass spectrometry, employing a nanoACQUITY UPLC (Waters, Milford, MA, USA) coupled to an Orbitrap XL (Thermo Electron, Bremen, Germany). The protocol described by Romero-Gavilán *et al.* [14] was followed. Each condition was analyzed in quadruplicate. Proteomic results were examined using PEAKS (Bioinformatics Solutions Inc., Waterloo, Canada). Functional classification of the identified proteins was performed using DAVID Go annotation (https://david.ncifcrf.gov/) and PANTHER programs (http://www.pantherdb.org/).

5.5. Statistical analysis

Physicochemical characterization and *in vitro* assay data, after evaluation of the normal distribution and equal variances, were submitted to one-way analysis of variance (ANOVA) with Tukey *post-hoc* test. Statistical analysis was performed using SigmaPlot v. 12.5 software for Windows (Systat Software Inc., Chicago, IL, USA). The differences between the MT materials and MT enriched with Zn were considered statistically significant at $p \leq 0.05$ (*), $p \leq 0.01$ (**), and $p \leq 0.001$ (***). Data were expressed as mean ± standard error (SE). For proteomic analysis, Student's *t*-test was performed, and protein adsorption differences were considered statistically significant at $p \leq 0.05$ and a ratio higher than 1.3 in either direction.

6. Acknowledgments

This work was supported by MINECO [MAT MAT2017-86043-R; RTC-2017-6147-1], Generalitat Valenciana [GRISOLIAP/2018/091], Universitat Jaume I under [UJI-B2017-37, Posdoc/2019/28], the University of the Basque Country under [GIU18/189] and Basque Government under [PRE_2017_2_0044]. The authors would like to thank Raquel Oliver, Jose Ortega and Iraide Escobés for their valuable technical assistance, and Antonio Coso (GMI-Ilerimplant) for producing the titanium discs.

7. References

[1] B. Dalisson, J. Barralet, *Adv. Healthc. Mater.* **2019**, *1900764*, 1.

[2] B. Pemmer, A. Roschger, A. Wastl, J. G. Hofstaetter, P. Wobrauschek, R. Simon, H. W. Thaler, P. Roschger, K. Klaushofer, C. Streli, *Bone* **2013**, *57*, 184.

[3] T. Huang, G. Yan, M. Guan, *Int. J. Mol. Sci.* **2020**, *21*, DOI 10.3390/ijms21041236.

[4] E. O'Neill, G. Awale, L. Daneshmandi, O. Umerah, K. W. H. Lo, *Drug Discov. Today* **2018**, *23*, 879.

[5] H. Yang, X. Qu, W. Lin, D. Chen, D. Zhu, K. Dai, Y. Zheng, *ACS Biomater. Sci. Eng.* **2019**, *5*, 453.

[6] H. Seo, Y. Cho, T. Kim, H. Shin, I. Kwun, *Nutr. Res. Pract.* **2010**, *4*, 356.

[7] N. Amin, C. C. T. Clark, M. Taghizadeh, S. Djafarnejad, *J. Trace Elem. Med. Biol.* **2020**, *57*, 126417.

[8] A. S. Prasad, *Adv. Nutr.* **2013**, *4*, 176.

[9] A. S. Prasad, *Front. Nutr.* **2014**, *1*, 1.

[10] A. S. Prasad, B. Bao, F. W. Beck, O. Kucuk, F. H. Sarkar, *Free Radic. Biol. Med.* **2004**, *37*, 1182.

[11] M. Jiménez, C. Abradelo, J. San Román, L. Rojo, *J. Mater. Chem. B* **2019**, *7*, 1974.

[12] Y. Su, I. Cockerill, Y. Wang, Y.-X. Qin, L. Chang, Y. Zheng, D. Zhu, *Trends Biotechnol.* **2019**, *37*, 428.

[13] A. Vishwakarma, N. S. Bhise, M. B. Evangelista, J. Rouwkema, M. R. Dokmeci, A. M. Ghaemmaghami, N. E. Vrana, A. Khademhosseini, *Trends Biotechnol.* **2016**, *34*, 470.

[14] F. Romero-Gavilán, A. M. Sanchez-Pérez, N. Araújo-Gomes, M. Azkargorta, I. Iloro, F. Elortza, M. Gurruchaga, I. Goñi, J. Suay, *Biofouling* **2017**, *33*, 676.

[15] J. Huang, Y. Yue, C. Zheng, *J. Biomed. Eng.* **1999**, *16*, 371.

[16] V. Nicolin, D. De Iaco, R. Valentini, *Ital. J. Anat. Embrylogy* **2016**, *121*, 37.

[17] F. Romero Gavilán, N. Araújo-Gomes, A. Cerqueira, I. Garcia Arnáez, C. Martínez Ramos, M. Azkargorta, I. Iloro, F. Elortza, M. Gurruchaga, J. Suay, et al., *JBIC J. Biol. Inorg. Chem.* **2019**, *24*, 563.

[18] M. M. Markiewski, B. Nilsson, K. N. Ekdahl, T. E. Mollnes, J. D. Lambris, *Trends Immunol.* **2007**, *28*, 184.

[19] N. Araújo Gomes, F. Romero Gavilán, Y. Zhang, C. Martinez Ramos, F. Elortza, M. Azkargorta, J. J. Martín de Llano, M. Gurruchaga, I. Goñi, J. J. J. P. Van Den Beucken, et al., *Colloids Surfaces B Biointerfaces* **2019**, *181*, 125.

[20] F. Romero-Gavilan, N. Araújo-Gomes, A. M. Sánchez-Pérez, I. García-Arnáez, F. Elortza, M. Azkargorta, J. J. M. de Llano, C. Carda, M. Gurruchaga, J. Suay, et al., *Colloids Surfaces B Biointerfaces* **2017**, *162*, 316.

[21] H. N. Kim, S. K. Lee, *Geochim. Cosmochim. Acta* **2013**, *120*, 39.

[22] M. J. Juan-Díaz, M. Martínez-Ibáñez, M. Hernández-Escolano, L. Cabedo, R. Izquierdo, J. Suay, M. Gurruchaga, I. Goñi, *Prog. Org. Coatings* **2014**, *77*, 1799.

[23] F. Romero-Gavilán, S. Barros-Silva, J. García-Cañadas, B. Palla, R. Izquierdo, M. Gurruchaga, I. Goñi, J. Suay, *J. Non. Cryst. Solids* **2016**, *453*, 66.

[24] J. C. Almeida, A. G. B. Castro, J. J. H. Lancastre, I. M. Miranda Salvado, F. M. A. Margaça, M. H. V. Fernandes, L. M. Ferreira, M. H. Casimiro, *Mater. Chem. Phys.* **2014**, *143*, 557.

[25] D. S. Brauer, E. Gentleman, D. F. Farrar, M. M. Stevens, R. G. Hill, *Biomed. Mater.* **2011**, *6*, 045007.

[26] M. Yamaguchi, M. Goto, S. Uchiyama, T. Nakagawa, *Mol. Cell. Biochem.* **2008**, *312*, 157.

[27] K. Yusa, O. Yamamoto, M. Iino, H. Takano, M. Fukuda, Z. Qiao, T. Sugiyama, *Arch. Oral Biol.* **2016**, *71*, 162.

[28] K. Janssens, P. Ten Dijke, S. Janssens, W. Van Hul, *Endocr. Rev.* **2005**, *26*, 743.

[29] Q. Gu, H. Yang, Q. Shi, *J. Orthop. Transl.* **2017**, *10*, 86.

[30] M. Giovanni, J. Yue, L. Zhang, J. Xie, C. N. Ong, D. T. Leong, *J. Hazard. Mater.* **2015**, *297*, 146.

[31] F. Romero-Gavilán, N. Araújo-Gomes, I. García-Arnáez, C. Martínez-Ramos, F. Elortza, M. Azkargorta, I. Iloro, M. Gurruchaga, J. Suay, I. Goñi, *Colloids Surfaces B Biointerfaces* **2019**, *174*, 9.

[32] T. E. Mollnes, M. Kirschfink, *Mol. Immunol.* **2006**, *43*, 107.

[33] N. H. Cho, S. Y. Seong, *Immunology* **2009**, *128*, 479.

[34] Z. Chen, T. Klein, R. Z. Murray, R. Crawford, J. Chang, C. Wu, Y. Xiao, *Mater. Today* **2016**, *19*, 304.

[35] D. I. Leavesley, A. S. Kashyap, T. Croll, M. Sivaramakrishnan, A. Shokoohmand, B. G. Hollier, Z. Upton, *IUBMB Life* **2013**, *65*, DOI 10.1002/iub.1203.

[36] R. M. Salasznyk, W. A. Williams, A. Boskey, A. Batorsky, G. E. Plopper, *J. Biomed. Biotechnol.* **2004**, *2004*, 24.

[37] C. Cho, S. Y. Jung, C. Y. Park, H. K. Kang, I. L. Yeo, B. Min, *Materials (Basel).* **2019**, *12*, 1.

[38] M. E. T. Hessenauer, K. Lauber, G. Zuchtriegel, B. Uhl, T. Hussain, M. Canis, S. Strieth, A. Berghaus, C. A. Reichel, *Acta Biomater.* **2018**, *82*, 24.

[39] J. Qi, L. Chi, S. Labeit, A. J. Banes, *Am. J. Physiol. - Cell Physiol.* **2008**, *295*, 975.

[40] G. Kalwitz, M. Endres, K. Neumann, K. Skriner, J. Ringe, O. Sezer, M. Sittinger, T. Häupl, C. Kaps, *Int. J. Biochem. Cell Biol.* **2009**, *41*, 649.

[41] B. S. Moonga, D. W. Dempster, *J Bone Min. Res* **1995**, *10*, 453.

[42] Y. X. Yin, C. Zhou, Y. P. Shi, Z. Z. Shi, T. H. Lu, Y. Hao, C. H. Liu, X. Wang, H. J. Zhang, L. N. Wang, *Mater. Sci. Eng. C* **2019**, *104*, 109896.

[43] J. Ma, N. Zhao, D. Zhu, *ACS Biomater. Sci. Eng.* **2015**, *1*, 1174.

[44] V. R. Samygina, A. V. Sokolov, G. Bourenkov, T. R. Schneider, V. A. Anashkin, S. O. Kozlov, N. N. Kolmakov, V. B. Vasilyev, *Metallomics* **2017**, *9*, 1828.

[45] E. Y. Karakas, A. Yetisgin, D. Cadirci, H. Sezen, R. Altunbas, F. Kas, M. Demir, T. Ulas, *J. Phys. Ther. Sci.* **2016**, *28*, 235.

[46] X. Liu, B. Zhang, J. D. McBride, K. Zhou, K. Lee, Y. Zhou, Z. Liu, J. X. Ma, *Diabetes* **2013**, *62*, 4228.

[47] L. Bing, Z. Sheng, C. Liu, L. Qian, Y. Wu, Y. Wu, G. Ma, Y. Yuyu, *Hum. Gene Ther.* **2019**, *30*, 339.

[48] J. Chao, P. Li, L. Chao, *Biol. Chem.* **2017**, *398*, 1309.

[49] J. Du, W. Feng, J. Sun, C. Kang, N. Amizuka, M. Li, *Sci. Rep.* **2016**, *6*, 1.

[50] X. Li, Z. Wu, J. Ni, Y. Liu, J. Meng, W. Yu, H. Nakanishi, Y. Zhou, *Oxid. Med. Cell. Longev.* **2016**, *2016*, DOI 10.1155/2016/7894247.

[51] J. Ni, Z. Wu, C. Peterts, K. Yamamoto, H. Qing, H. Nakanishi, *J. Neurosci.* **2015**, *35*, 12488.

[52] B. Tong, B. Wan, Z. Wei, T. Wang, P. Zhao, Y. Dou, Z. Lv, Y. Xia, Y. Dai, *Clin. Exp. Immunol.* **2014**, *177*, 586.

[53] S. W. Cox, B. M. Eley, M. Kiili, A. Asikainen, T. Tervahartiala, T. Sorsa, *Oral Dis.*

2006, *12*, 34.

[54] F. Romero-Gavilán, N. C. Gomes, J. Ródenas, A. Sánchez, F. , Mikel Azkargorta, Ibon Iloro, I. G. A. Elortza, M. Gurruchaga, I. Goñi, and J. Suay, *Biofouling* **2017**, *33*, 98.

[55] M. Martinez-Ibañez, M. J. Juan-Diaz, I. Lara-Saez, A. Coso, J. Franco, M. Gurruchaga, J. Suay Anton, I. Goñi, *J. Mater. Sci. Mater. Med.* **2016**, *27*, DOI 10.1007/s10856-016-5690-9.

[56] International Organization for Standardization, **2009**, *3 ED*, 42.

[57] International Organization for Standardization, **2012**.

[58] A. Cerqueira, F. Romero-Gavilán, N. Araújo-Gomes, I. García-Arnáez, C. Martinez-Ramos, S. Ozturan, M. Azkargorta, F. Elortza, M. Gurruchaga, J. Suay, et al., *Mater. Sci. Eng. C* **2020**, *116*, 111262.

Figures

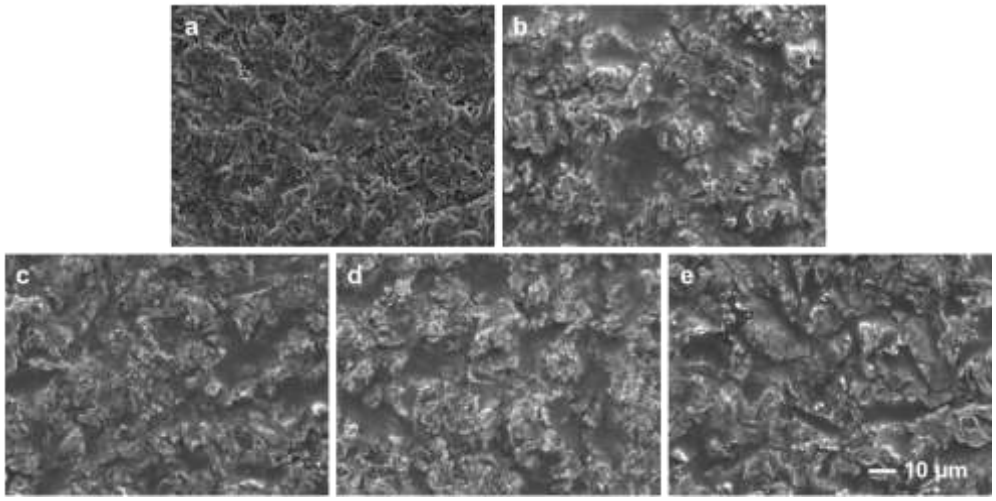

Figure 1. SEM microphotograph of SAE-Ti (a), MT (b), MT0.5Zn (c), MT1Zn (d) and MT1.5Zn (e). Scale bar, 10 µm.

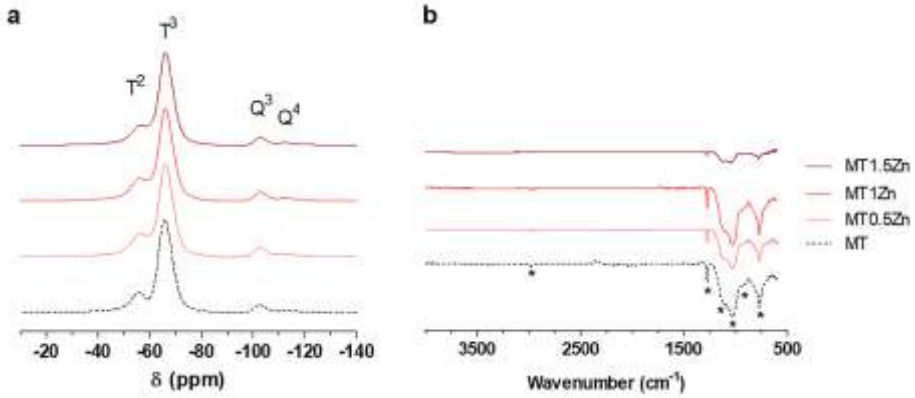

578

579 **Figure 2**. ^{29}Si MAS-NMR (a) and FTIR (b) spectra of sol-gel networks MT, 0.5MTZn, MT1Zn,
580 and MT1.5Zn.

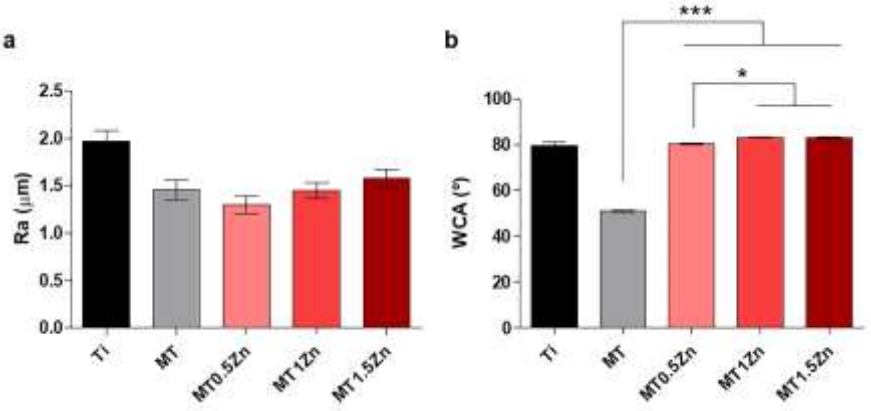

581

582 **Figure 3.** The arithmetic average of roughness (Ra; a) and contact angle (WCA; b). Results are
583 shown as mean ± SE. The asterisks ($p \leq 0.05$ (*) and $p \leq 0.001$ (***)) indicate the statistical
584 significance of differences between the materials with and without Zn (MT).

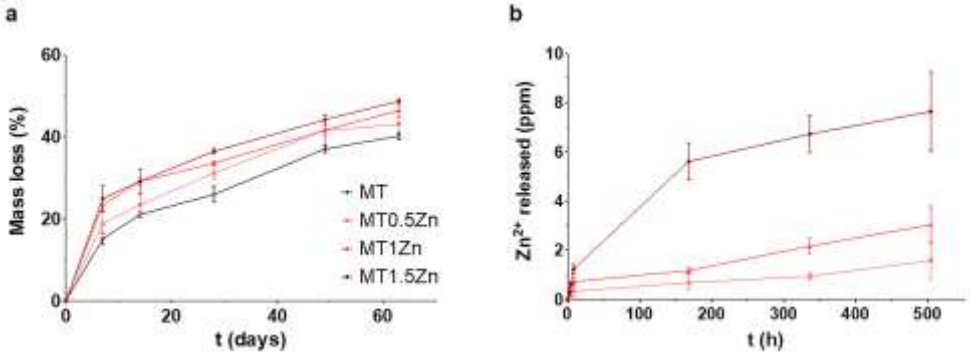

585

586 **Figure 4.** Hydrolytic degradation (a) and Zn^{2+} release kinetics (b) for the MT sol-gels doped
587 with $ZnCl_2$. Bars indicate standard errors.

588

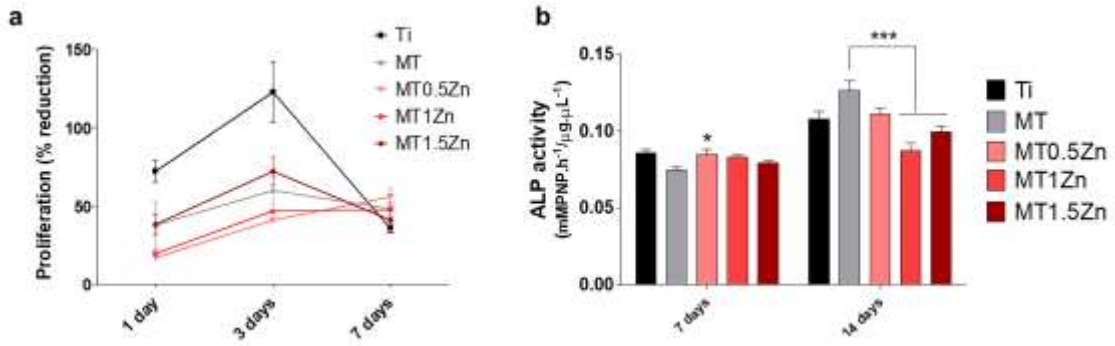

589

590 **Figure 5.** MC3T3-E1 (a) cell proliferation after 1, 3, and 7 days and (b) ALP activity after 7
591 and 14 days. Results are shown as mean ± SE. The asterisks ($p \leq 0.05$ (*) and $p \leq 0.001$ (***))
592 indicate statistically significant differences between the materials with Zn and the coating
593 without Zn (MT).

594

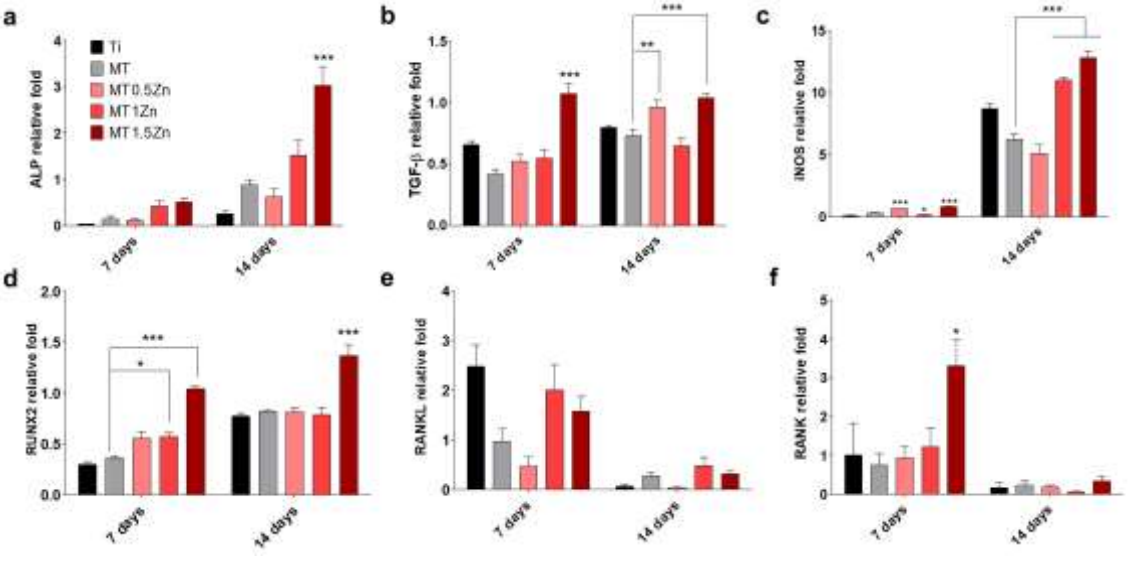

595

596 **Figure 6.** Gene expression of (a) ALP, (b) TGFβ, (c) iNOS, (d) RUNX2, (e) RANKL, and (f)
597 RANK in MC3T3-E1 cells at 7 and 14 days of assay. Results are shown as mean ± SE. The
598 asterisks ($p \leq 0.05$ (*), $p \leq 0.01$ (**), and $p \leq 0.001$ (***)) indicate statistically significant
599 differences between the materials with Zn and the coating without Zn (MT). Data were
600 normalized to blank wells (without any material).

601

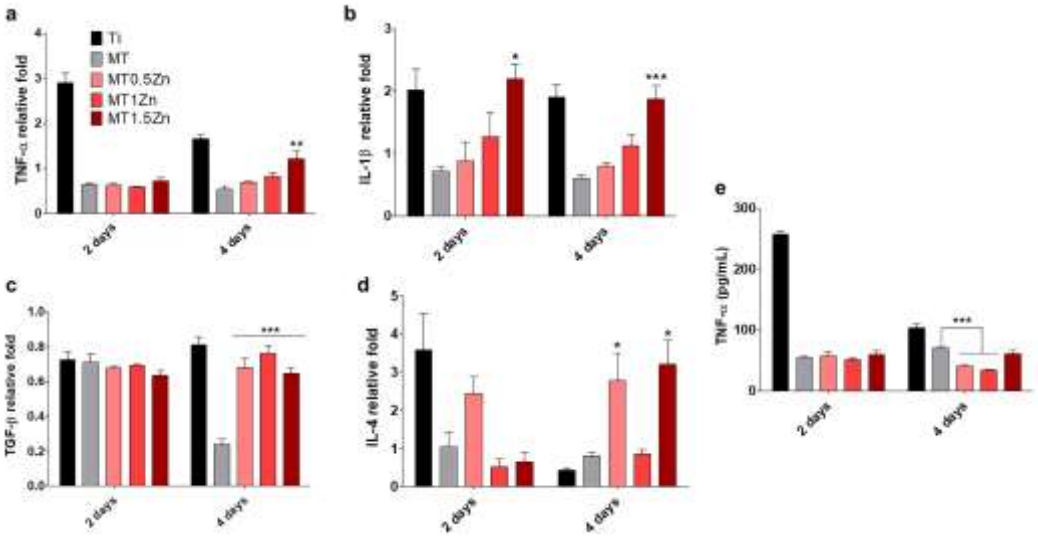

Figure 7. Gene expression of (a) TNFα, (b) IL-1β, (c) TGF-β, and (d) IL-4, and (e) TNF-α cytokine liberation in RAW264.7 cells at 2 and 4 days of assay. Results are shown as mean ± SE. The asterisks ($p \leq 0.05$ (*), $p \leq 0.01$ (**), and $p \leq 0.001$ (***)) indicate statistically significant differences between the materials with Zn and the coating without Zn (MT). Gene expression data were normalized to blank wells (without any material).

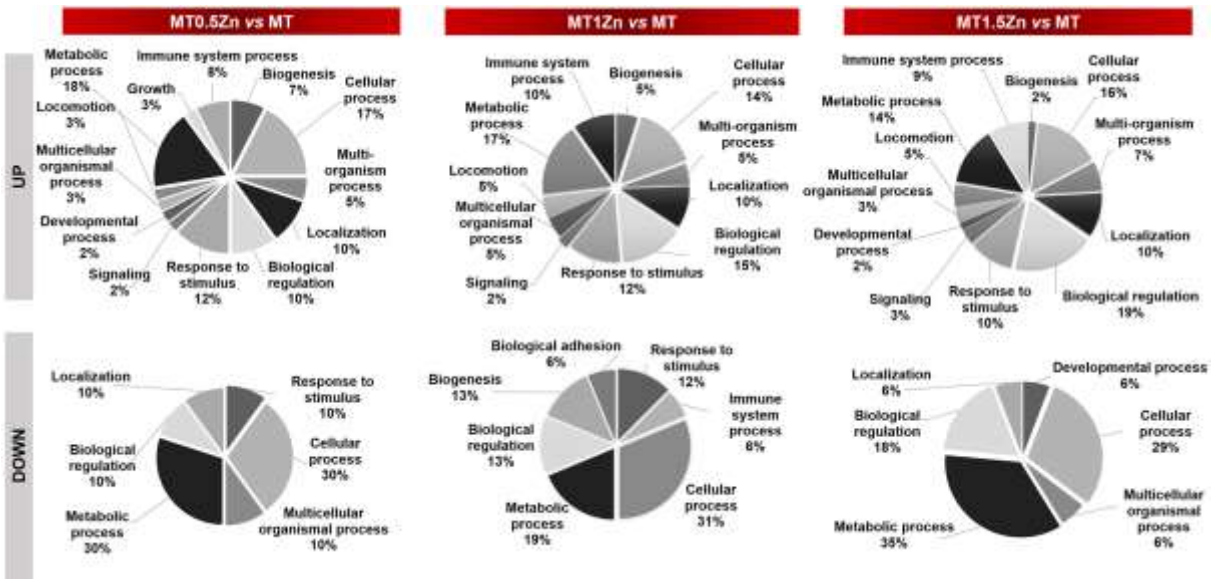

Figure 8. PANTHER functional classification of proteins differentially adsorbed onto the Zn-containing coatings in comparison with the control material MT. Proteins with $p \leq 0.05$ and a ratio higher than 1.3 in either direction (UP – increased and DOWN – reduced) were considered differentially adsorbed.

Tables

Table 1. Proteins with important functions in the bone tissue regeneration process differentially adsorbed onto the Zn-containing coatings. Proteins with $p \leq 0.05$ and a ratio higher than 1.3 in either direction (UP: increased and DOWN: reduced) were considered differentially adsorbed.

		MT0.5Zn vs MT	MT1Zn vs MT	MT1.5Zn vs MT
Immune responses	**UP**	FHR1, IGJ, SAMP, CO4A, CLUS, LAC3, C1S, IGKC	IGJ, SAMP, CO4A, CLUS, CO3, CO4B	FHR1, IGJ, SAMP, CO4A, CO9, CXCL7, CLUS, CO3, IC1
	DOWN	-	-	-
Apolipoproteins	**UP**	APOF, APOL1, SAA4, APOC4, APOC3, APOC2	APOF, APOL1, SAA4, APOA2, APOA1	APOF, APOL1, SAA4, APOC4, APOC2, APOA2
	DOWN	-	-	-
Blood coagulation	**UP**	HBB	PLF4, PROC, HBB	PLF4, IPSP
	DOWN	HRG	-	-
Osteogenesis	**UP**	VTNC	VTNC, TITIN	CERU, VTNC, KAIN
	DOWN	TITIN	PRDX1	CATB

Table 2. Targets studied in MC3T3-E1 and RAW264.7.

Gene	Accession	Sequence	Product length
GADPH	XM_017321385	F: TGCCCCCATGTTTGTGATG R: TGGTGGTGCAGGATGCATT	83
ALP	XM_006538499	F: CGGGACTGGTACTCGGATAA R: ATTCCACGTCGGTTCTGTTC	157
TGFβ	NM_011577	F: TTGCTTCAGCTCCACAGAGA R: TGGTTGTAGAGGGCAAGGAC	183
iNOS	NM_001313922	F: CACCTTGGAGTTCACCCAGT R: ACCACTCGTACTTGGGATGC	170
RUNX2	NM_001271631	F: CCCAGCCACCTTTACCTACA R: TATGGAGTGCTGCTGGTCTG	150
RANKL	AF019048	F: AGCCGAGACTACGGCAAGTA R: GCGCTCGAAAGTACAGGAAC	208
RANK	AF019046	F: GCTGGCTACCACTGGAACTC R: GTGCAGTTGGTCCAAGGTTT	182
TNF-α	NM_001278601	F: AGCCCCCAGTCTGTATCCTT R: CTCCCTTTGCAGAACTCAGG	212
IL-1β	NM_008361	F: GCCCATCCTCTGTGACTCAT	230

IL-4	NM_021283	R: AGGCCACAGGTATTTTGTCG F: TCAACCCCCAGCTAGTTGTC R: TGTTCTTCGTTGCTGTGAGG	177

640

641

642

643

644

645

646

647 **Table of Contents**

648 New Zn-doped sol-gel coatings were developed. These coatings could improve bone
649 regeneration capacity in a Zn dose-dependent manner and exert an anti-inflammatory effect. A
650 correlation between protein adsorption patterns and cellular response were established. This
651 new knowledge can be of great use to understand the role of Zn in tissue regeneration when it
652 is introduced to a biomaterial.

653

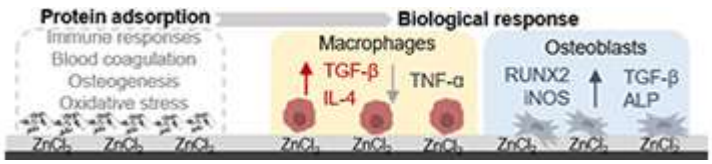

654

655

656

657

658